Progress in Oceanography 176 (2019) 102126

Contents lists available at ScienceDirect

Progress in Oceanography

journal homepage: www.elsevier.com/locate/pocean

The biogeochemical impact of glacial meltwater from Southwest Greenland

Katharine R. Hendry [a,*], Veerle A.I. Huvenne [b], Laura F. Robinson [a], Amber Annett [c], Marcus Badger [d], Allison W. Jacobel [e,f], Hong Chin Ng [a], Jacob Opher [g,h,i], Rebecca A. Pickering [j,k], Michelle L. Taylor [l], Stephanie L. Bates [a], Adam Cooper [c], Grace G. Cushman [e], Claire Goodwin [m], Shannon Hoy [n], George Rowland [a], Ana Samperiz [a,o], James A. Williams [o], Eric P. Achterberg [p], Carol Arrowsmith [q], J. Alexander Brearley [g], Sian F. Henley [r], Jeffrey W. Krause [j,k], Melanie J. Leng [q,s], Tao Li [a], Jerry F. McManus [e], Michael P. Meredith [g], Rupert Perkins [o], E. Malcolm S. Woodward [t]

[a] School of Earth Sciences, University of Bristol, Wills Memorial Building, Queen's Road, Bristol BS8 1RJ, UK
[b] National Oceanography Centre, University of Southampton Waterfront Campus, European Way, Southampton SO14 3ZH, UK
[c] Ocean and Earth Science, University of Southampton, Waterfront Campus, European Way, Southampton SO14 3ZH, UK
[d] School of Environment, Earth & Ecosystem Sciences, The Open University, Walton Hall, Milton Keynes MK7 6AA, UK
[e] Lamont-Doherty Earth Observatory, Columbia University, 61 US-9W Palisades, NY 10964, USA
[f] Environment and Society, Brown University, 85 Waterman Street, Providence, RI 02912, USA
[g] British Antarctic Survey, High Cross, Madingley Road, Cambridge CB3 0ET, UK
[h] Centre for Ocean and Atmospheric Sciences, School of Environmental Sciences, University of East Anglia, Norwich Research Park, Norwich NR4 7TJ, UK
[i] Centre for Environment Fisheries and Aquaculture Science, Pakefield Road, Lowestoft, Suffolk NR33 0HT, UK
[j] Dauphin Island Sea Laboratory, 101 Bienville Boulevard, Dauphin Island, AL 36528, USA
[k] University of South Alabama, Mobile, AL 36688, USA
[l] School of Biological Sciences, University of Essex, Wivenhoe Park, Colchester CO4 3SQ, UK
[m] Huntsman Marine Science Centre, 1 Lower Campus Rd, Saint Andrews, NB E5B 2L7, Canada
[n] Center for Coastal & Ocean Mapping/Joint Hydrographic Center, Jere A. Chase Ocean Engineering Lab, 24 Colovos Road, Durham, NH 03824, USA
[o] School of Earth and Ocean Sciences, Cardiff University, Main Building, Park Place, Cardiff CF10 3AT, UK
[p] GEOMAR Helmholtz Centre for Ocean Research, Kiel, Wischhofstraße 1-3, D-24148 Kiel, Germany
[q] NERC Isotope Geosciences Facility, British Geological Survey, Keyworth, Nottingham NG12 3GG, UK
[r] School of GeoSciences, University of Edinburgh, James Hutton Road, Edinburgh EH9 3FE, UK
[s] Centre for Environmental Geochemistry, School of Biosciences, Sutton Bonington Campus, University of Nottingham, Loughborough LE12 5RD, UK
[t] Plymouth Marine Laboratory, Prospect Place, The Hoe, Plymouth PL1 3DH, UK

ARTICLEINFO

Keywords:
Biogeochemistry
Nutrients
Glaciers
Primary production
Silica cycling

ABSTRACT

Biogeochemical cycling in high-latitude regions has a disproportionate impact on global nutrient budgets. Here, we introduce a holistic, multi-disciplinary framework for elucidating the influence of glacial meltwaters, shelf currents, and biological production on biogeochemical cycling in high-latitude continental margins, with a focus on the silica cycle. Our findings highlight the impact of significant glacial discharge on nutrient supply to shelf and slope waters, as well as surface and benthic production in these regions, over a range of timescales from days to thousands of years. Whilst biological uptake in fjords and strong diatom activity in coastal waters maintains low dissolved silicon concentrations in surface waters, we find important but spatially heterogeneous additions of particulates into the system, which are transported rapidly away from the shore. We expect the glacially-derived particles – together with biogenic silica tests – to be cycled rapidly through shallow sediments, resulting in a strong benthic flux of dissolved silicon. Entrainment of this benthic silicon into boundary currents may supply an important source of this key nutrient into the Labrador Sea, and is also likely to recirculate back into the deep fjords inshore. This study illustrates how geochemical and oceanographic analyses can be used together to probe further into modern nutrient cycling in this region, as well as the palaeoclimatological approaches to investigating changes in glacial meltwater discharge through time, especially during periods of rapid climatic change in the Late Quaternary.

* Corresponding author.
E-mail address: K.Hendry@bristol.ac.uk (K.R. Hendry).

https://doi.org/10.1016/j.pocean.2019.102126
Received 3 October 2018; Received in revised form 5 April 2019; Accepted 15 June 2019
Available online 17 June 2019

1. Introduction

The high-latitude regions are experiencing some of the most rapid environmental changes observed globally in recent decades. This is particularly true for the Arctic. Here, temperatures are rising twice as fast as the global mean, the Nordic Seas are warming at an accelerated rate (Alexeev et al., 2017), Arctic sea-ice is thinning and moving faster (Lindsay and Schweiger, 2015), and multi-year Arctic sea-ice is declining (Maslanik et al., 2007), with significant implications for the interaction between the atmosphere and the oceans (Provost et al., 2017). The Greenland Ice Sheet (GrIS) is experiencing significant mass loss largely through surface melting but also via ice discharge at glacier fronts (Enderlin et al., 2014; Felikson et al., 2017; van den Broeke et al., 2017). This melting is likely to have a global impact: the North Atlantic receives freshwater from the Nordic Seas, GrIS, and the Canadian Arctic (Bamber et al., 2018), which influences the density structure, circulation, and stratification in regions where deep water-masses form; these represent a major component of ocean circulation that drives global fluxes of heat and freshwater (Carmack et al., 2016; Proshutinsky et al., 2015; Yang et al., 2016). In addition to freshwater budgets, there has been increasing focus on the role of glaciers and ice sheets in supplying organic material and inorganic nutrients to marine systems. There are significant fluxes of nutrients in GrIS runoff both in dissolved and particulate form, including nitrogen (Wadham et al., 2016), phosphate (Hawkings et al., 2016), dissolved silicon (Hawkings et al., 2017; Meire et al., 2016), and iron (Bhatia et al., 2013; Hawkings et al., 2014). The extent to which these nutrients reach the coastal oceans, and are subsequently advected or mixed from the continental shelves into the open oceans via boundary currents, is poorly constrained and a matter of debate (Hopwood et al., 2015). Both dissolved nutrient and particulate dynamics are significantly impacted by circulation processes (Hopwood et al., 2015) and biological activity within glacially-influenced fjords. These regions could be a significant trap of dissolved inorganic phases (Meire et al., 2017), and have the potential to prevent the nutrient-rich glacial waters reaching the coastal seas. Despite this possibility, distal summer phytoplankton blooms have been detected off Southwest Greenland in association with glacial melt (Arrigo et al., 2017) and ecosystem models indicate sensitivity to meltwater input (Oliver et al., 2018). An understanding of how natural resources – including fisheries, bird, and mammal stocks that are essential for food and encouraging tourism – will respond in the future to increasing anthropogenic stress on a regional and global scale relies on an understanding of foundational processes of these ecosystem services, including marine biogeochemistry and the sources and sinks of essential nutrients (Berthelsen, 2014; Meire et al., 2017; Weatherdon et al., 2016).

The overarching goal of the Isotope Cycling in the Labrador Sea (ICY-LAB; icylab.wordpress.com) study is to understand the cycling of nutrients in the climatically critical but understudied regions of the Labrador Sea and Greenland fjords. The approach of ICY-LAB is to capture the whole biogeochemical system in these areas of marked environmental change using carefully planned field sampling strategies, with research expeditions to coastal Greenland and the open ocean Labrador Sea. The principal dataset was collected during an oceanic expedition on the RRS *Discovery* (DY081, July-August 2017), with the aim to investigate the influence of glacial meltwater on nutrient cycling in the shelf seas off SW Greenland. Particular focus was placed on the silica budget and how this is framed within the oceanographic and biological processes acting on the West Greenland margin. Uniquely, we combined a range of both traditional and novel methodologies to detect and trace meltwater and glacial material from the shelf across the slope, and to investigate the biogeochemical and biological impact of these inputs. Bringing these different approaches together is essential in these margin environments to obtain a full picture of biogeochemical cycling, providing a robust insight into the system over a range of spatial and temporal scales that are otherwise challenging to resolve (Fig. 1).

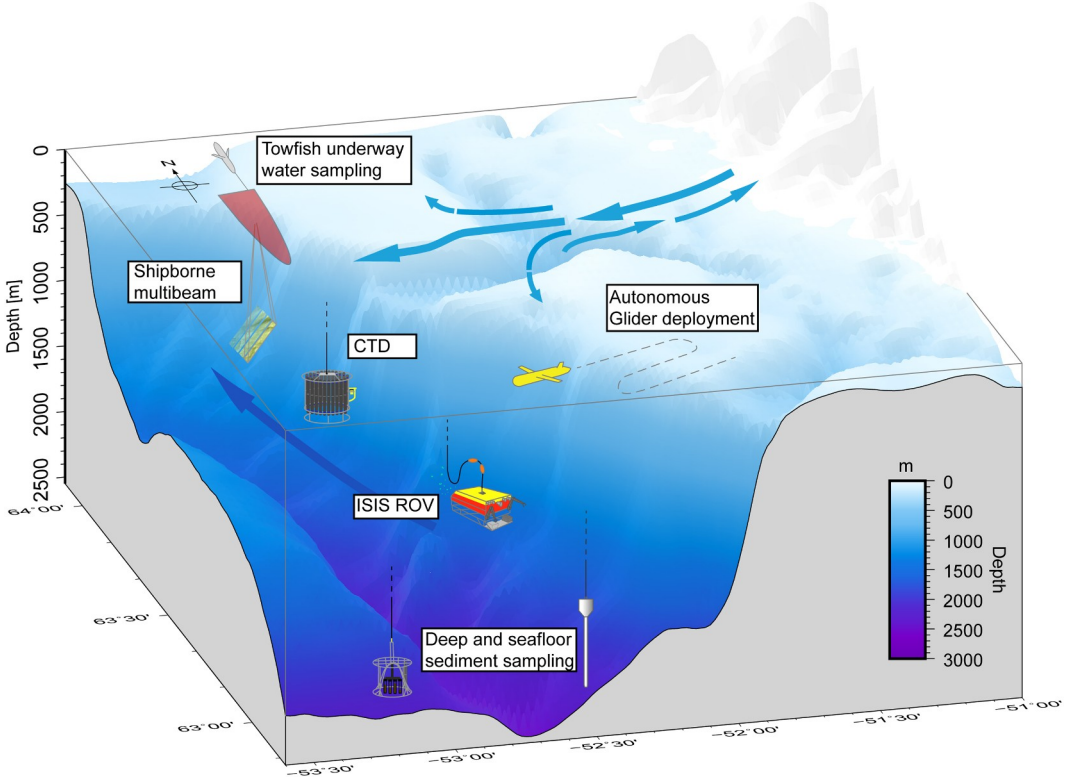

Fig. 1. Summary figure showing the multi-discipline approach taken during expedition DY081 of project ICY-LAB.

2. Methods and materials

2.1. Fieldwork rationale

The data presented in this paper were collected during expedition DY081, centred on the coastal shelf and slope regions off Southwest Greenland. Model results indicate that this region is influenced by surface meltwater from the Western GrIS, in addition to a significant input of freshwater delivered from the Eastern GrIS via the strong East Greenland Current (EGC) (Luo et al., 2016). The study locations were selected to represent this conduit to the open ocean for glacial runoff from the Western and Southwestern GrIS, which have been the focus of recent terrestrial studies carried out in collaboration with the Bristol Glaciology Centre (Hawkings et al., 2018; Hawkings et al., 2017). Full details of the oceanographic setting are given in Appendix A.

We selected the main study location for the ICY-LAB project ("Gothåb (Nuuk) Trough", Fig. 2a) to be adjacent to Nuuk, which has experienced increasing glacial run-off in recent years (Van As et al., 2014). During DY081, Southern Greenland was strongly influenced by both icebergs and sea ice, but two sites ("Narsaq" and "Cape Farewell", Fig. 2a) were still selected there for providing glacial troughs that could act as direct comparisons to the further north Nuuk site further north. Orphan Knoll, on the western margin of the Labrador Sea, was selected as a distal comparison site, and for complementary palaeoclimate, biological and habitat mapping studies (Fig. 2a).

The unique holistic observational approach we took is illustrated in Fig. 1, and included (a) initial bathymetric mapping using acoustic methods (multibeam echosounders) to increase our understanding of the local terrain and to enable accurate planning of further sampling activities; (b) characterisation of the water column structure using CTD casts and glider deployments; (c) sampling of surface and bottom waters for biogeochemical analyses using the CTD rosette and a trace metal clean towfish; (d) sampling of seabed sediments using a megacorer (for geochemical studies of pore waters) and gravity corer (for palaeoceanographic investigations); (e) seabed observations and precision sampling for biological, palaeoceanographic and sedimentological studies using a work-class scientific ROV.

2.2. On-board methodologies and additional laboratory techniques

2.2.1. Mapping and acoustics

During DY081, multiple acoustic systems were deployed on the ship (e.g. EM122 multibeam echosounder (12 kHz); EM710 multibeam echosounder; SBP120 sub-bottom echosounder (2.5–6.5 kHz)). These were coordinated via a K-Sync system to avoid interference and cross-talk.

Bathymetry data were processed on-board with the Caris HIPS & SIPS software v.8, using standard settings and procedures (data import, navigation and attitude check, application of a "zero tide", gridding into a 25 m × 25 m pixel BASE surface). Backscatter data were processed with Fledermaus FMGT, again using default settings.

2.2.2. Physical oceanography

High-resolution water column studies surrounding the prominent glacial Gothåb (Nuuk) Trough were carried out utilising both a grid of Conductivity Temperature Depth (CTD) casts and the deployment of two 1000 m-rated Slocum gliders (Fig. 2). CTD casts were also used at the south Greenland and Orphan Knoll study sites. Hydrographic

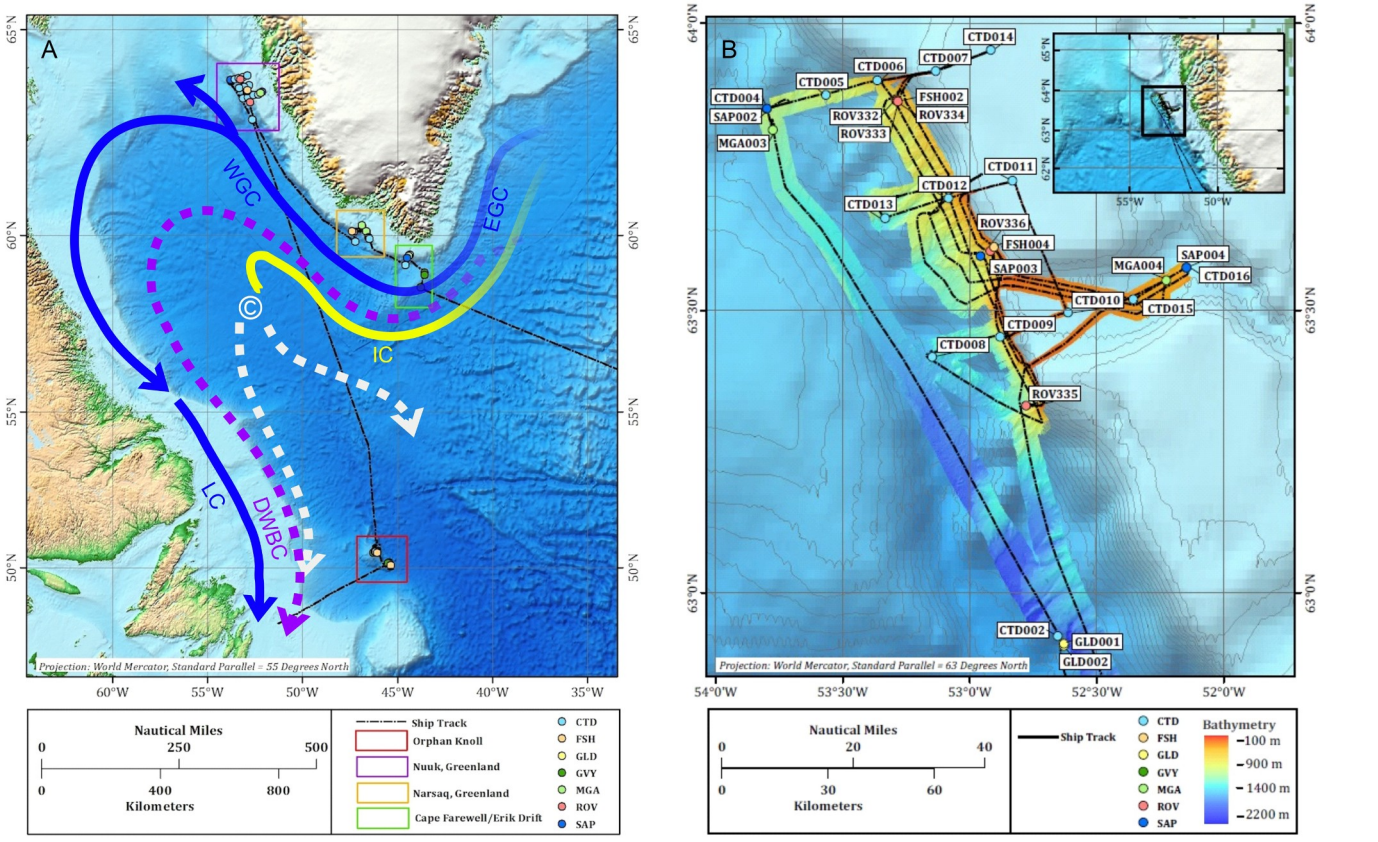

Fig. 2. (A) Map showing route and main working areas of expedition DY081. Produced in Mercator projection with a standard parallel of 55˚N. Arrows show the main current systems in the Labrador Sea: Irminger Current (IC in yellow), West and East Greenland Currents and Labrador Current (WGC, EGC, LC in blue), and the Deep Western Boundary Current (DWBC). Cold, deep polar overflow waters are represented by the purple arrow. The main site of deep-water convection is marked by C, and represented by white arrows. (B) Map of Nuuk grid location with ship track, bathymetry and station locations. Produced in Mercator projection with a standard parallel of 63˚N. (For interpretation of the references to colour in this figure legend, the reader is referred to the web version of this article.)

analysis enabled characterization of the water column structure in each study location, specifically to locate and quantify the freshwater inputs at the Greenland sites. Salinity was calibrated using bottle samples collected at discrete depths. After laboratory calibration of these samples, no drift corrections were required. Overall errors for temperature were 0.0006 °C (based on laboratory calibration) and 0.002 for salinity. Prior to analysis, data from these stations were gridded to a vertical and horizontal resolution of 10 m and 6 km respectively.

Vessel Mounted Acoustic Doppler Current Profilers (VMADP at 75 and 150 kHz; Teledyne RD instruments) were secured onto the drop keel in surface waters near the centre-line and beneath the *RRS Discovery*, and used to measure the horizontal current velocity profile. Bottom tracking data were only collected from the 150 kHz instrument intermittently between 18th July and 24th July 2017 while close to Nuuk. In addition, downward and upward looking lowered 300 kHz ADCPs (LADCPs) were mounted on the CTD rosette. LADCP data were processed using LDEO LADCP processing software version IX_8, run on Matlab. Full details of the other sensors attached to the CTD rosette and gliders can be found elsewhere (Hendry, 2017).

2.2.3. Biogeochemistry and chemical oceanography

2.2.3.1. Water column. Water column samples were collected using Niskin bottles attached to the CTD rosette (10L volume) and the Remotely Operated Vehicle (ROV) *Isis* (4 L volume), and via a trace-metal clean towfish. The towfish system comprised of a weighted titanium bodied fish lowered into the water at the stern and streamed as far from the ship as possible. When towed it was at approximately 2 m depth, and water was pumped into the ship's labs through an ultra-clean pump and tubing. Trace-metal sampling was only carried out when the ship was moving at speeds greater than 0.5 knots in order to avoid contamination from the hull of the vessel. Four stand-alone pumps (SAPs) were also deployed at key locations to collect water column particles.

Samples of seawater were collected for inorganic macronutrients, water oxygen isotope composition ($\delta^{18}O$) and carbonate chemistry parameters (pH, alkalinity), which are used for investigating freshwater input in high-latitude regions (Hendry et al., 2018; Meredith et al., 2008; Thomas et al., 2011). Phytoplankton pigments were analysed on board, and compared to sensor-derived fluorescence data, to assess algal standing stocks in relation to meltwater input. Full details of sampling methods and laboratory techniques are available in Appendix B.

2.2.3.2. Diatom productivity. Biogenic silica ($bSiO_2$) production (i.e. diatom productivity) analyses were done using radioisotope ^{32}Si as detailed in Krause et al. (2011). Briefly, samples were collected within the euphotic zone (sample depths based on light and relative to irradiance just below the surface) and dispensed into acid-cleaned 125 mL polycarbonate bottles. 322 Bq of $^{32}Si(OH)_4$ was added to each sample, and bottles were incubated on deck in surface-seawater-cooled incubators covered with neutral density screening to mimic the depth of collection. After incubation, samples were filtered through 1.2 µm pore size polycarbonate membrane filters. Particulate ^{32}Si activity was quantified using a GM-25 Multicounter (Risø DTU National Laboratory, Denmark) after the samples had aged into secular equilibrium with the short-lived daughter isotope, ^{32}P.

2.2.3.3. Radium isotopes.To investigate the fate of solutes sourced from benthic sediments or glacial meltwater, large-volume surface samples for radium (Ra) isotope analysis were collected from the trace-metal clean towfish system, both when the ship was underway (~2m water depth) and stationary (~5m water depth). A total of 200–300 L of seawater from a single sampling event were then passed through a plastic column holding MnO_2-coated acrylic fibre, which quantitatively binds Ra in the sample. The fibers and adsorbed Ra isotopes were then rinsed with deionized water (Milli-Q, Millipore), dried to an appropriate moisture content and loaded into a Ra Delayed Coincidence Counter (RaDeCC; Scientific Computer Instruments, USA) so as to quantify ^{223}Ra and ^{224}Ra content following the methods of Moore and Arnold (1996) and Moore (2008). Each sample was counted 4 times over ~4 months to determine the activities of excess ^{224}Ra and ^{223}Ra, above the activities supported by their parent isotopes in the water column (^{228}Th and ^{227}Ac, respectively). Detector efficiencies were determined and monitored regularly at sea and in the laboratory with standards (Annett et al., 2013). Final reported activities have been corrected for any decay that occurred between sample collection and analysis, activity supported by parent isotopes, detector background, and efficiency.

2.2.3.4. Sediment-water interface. High-latitude ocean margin sediments are increasingly being recognised as an important source of inorganic nutrients and key elements (Henley et al., 2018; Kuzyk et al., 2017; Sherrell et al., 2018). To investigate the role of sediments in these glacially-influenced shelf and slope environments, we collected pore-fluid samples at coastal Greenland and the Labrador Sea. Short sediment cores (≤40 cm) were acquired from the study area with a mega corer. Using Rhizon filters (0.15 µm, Rhizosphere Research Products), pore water was extracted from the sediment cores and filtered into syringes, and the samples were stored under cool conditions prior to analysis. Pore water dissolved silicon concentrations were analysed on-board and post-expedition using a V-1200 Vis spectrophotometer, employing a standard molybdate-blue methodology (using Hach Lange reagents). The samples were corrected for blank and calibrated against a ten-point curve that was developed using Si standards of known concentrations. In addition to mega-cores, we also employed ROV push cores to obtain short sediment cores for pore-fluid sampling, in regions where complex bathymetry or the presence of ice-rafted material precluded the use of a megacorer.

2.2.4. Palaeoclimate

Two samples types were collected for palaeoclimate research – fossil deep-sea corals and sediment cores. ROV operations were the primary tool for benthic biological and fossil coral collections using grab or suction devices. In addition, where large fossil coral graveyards were observed, a net was used to sample fossil corals. Gravity cores were also collected to obtain long-term records of changes in meltwater flux and iceberg dynamics over the Late Quaternary, thereby providing a longer-term temporal context to the broader data set. Megacores, collected primarily for biogeochemical studies, were also subsampled to provide core-top material that could potentially replace any sections lost from the gravity cores during retrieval.

2.3. Mass balance calculations

To calculate the freshwater mass balance in the study area, the seawater samples are presumed to comprise a mixture of three source water end-members: ocean, sea ice melt and meteoric water, which is assumed to be dominated by glacial discharge. The three end-member assumption enables quantification of the freshwater fractions via the following mass balance equations (Meredith et al., 2001):

$$F_{ir} + F_{me} + F_{si} = 1$$

$$F_{ir}S_{ir} + F_{me}S_{me} + F_{si}S_{si} = S_{ms}$$

$$F_{ir}\delta_{ir} + F_{me}\delta_{me} + F_{si}\delta_{si} = \delta_{ms}$$

where F_{ir}, F_{me}, F_{si} are the calculated fractions of Irminger Water, meteoric and sea ice melt respectively (Irminger Water being the chosen ocean endmember), which sum to 1 by definition. The result is clearly dependent on the exact choice of endmembers for salinity (S_{ir}, S_{me}, S_{si}) and $\delta^{18}O$ (δ_{ir}, δ_{me}, δ_{si}) for the Irminger Water, meteoric and sea ice melt respectively. S_{ms} and δ_{ms} are the measured salinity and $\delta^{18}O$ of each sample.

Properties for the sea ice melt and meteoric endmembers (Table 1) were based on values reported in Dodd et al. (2009), Melling and Moore (1995), Meredith et al. (2001), and the CTD observations from the DY081 research cruise. Note that negative sea ice melt percentages reflect a net sea ice formation from the water parcel sampled.

3. Results

EM-122 multibeam swath bathymetry datasets (e.g. Fig. 2) are now published on PANGAEA (doi: https://doi.org/10.1594/PANGAEA.892825). The full water column data from CTD profiles and bottles (hydrography, oxygen isotopes, carbonate chemistry, macronutrients e.g. Fig. 3) are published on PANGAEA (doi.pangaea.de/https://doi.org/10.1594/PANGAEA.896544). Here we present a subset of the results, focusing on characterisation of the silica cycle in the water column and sediments.

3.1. Silica cycling parameters in the water column and sediments

3.1.1. Water column macronutrients and pigments

The nearshore macronutrient concentrations were typically low (< 11 μM nitrate, < 0.2 μM nitrite, < 0.75 μM phosphate and < 5 μM DSi in the upper 50 m of the water column) reaching minima in the surface waters with lowest salinity and lowest $\delta^{18}O$ (an example of which is given in Fig. 3a, see also Appendix C). Sections of CTD macronutrient and pigment bottle data from the Nuuk grid, integrated over the top 50 m, reveal consistent onshore-offshore trends (an example of which is given in Fig. 3b, see also Appendix C). Integrated macronutrient concentrations decreased towards shore concurrent with an increase in Si:N. Integrated Chl *a* increased towards shore, indicative that at least some of the macronutrient decrease is a result of biological uptake into biomass. However, the ratio of Chl *a*:Chl *c* peaked at the shelf break, and then decreased again towards shore, indicating a lower diatom proportional contribution to biomass in the same locations as the lowest integrated water column DSi (Fig. 3b, see also Appendix C).

3.1.2. Diatom productivity

Surface $bSiO_2$ production among the three sampling regions ranged from 0.05 to 0.31 μmol Si L^{-1} d^{-1} (Fig. 4). For the most part, rates declined with depth; however, the Orphan Knoll site had subsurface maxima at the 20% isolume (~10–20 m) and base of the euphotic zone (i.e. 1% isolume, 20–50 m). The production rates of $bSiO_2$ among the Nuuk profiles were typically higher than Orphan Knoll and Southern Greenland (Fig. 4); however, samples incubated in the dark (collected from below the euphotic zone) in Nuuk still had measurable production.

3.1.3. Sediment dissolved silicon profiles

Pore water DSi collected from the mega cores and the ROV push cores from the Labrador Sea and coastal Greenland during DY081 expedition range from 49 to 616 μM (Fig. 5). All cores generally show an initial increase in pore water DSi with core depth, indicating supply of Si to bottom waters from the sediment via dissolution. At greater depths, the rates of increase of pore water DSi with depth slow down or even reverses (Fig. 5).

There is good agreement between pore water DSi results (Fig. 5) observed in ROV push cores and mega cores from Orphan Knoll and South Greenland (off Narsaq and Cape Farewell). To the best of our knowledge, this is the first formal comparison of pore water DSi profiling using ROV push cores compared to megacorers, and our results provide confidence to the application of this sampling methodology in future studies, especially in settings where the use of a megacorer proves to be challenging (e.g. complex bathymetry, presence of coarse ice-rafted material). In contrast, there is larger variation in pore water DSi (Fig. 5) among the sites off Nuuk (Appendix C), which could in part be related to the greater variability in sediment composition (e.g. ice-rafted debris, fossil fragments) and characteristics (e.g. grain size) observed at these sites. More importantly, the highest pore water DSi concentrations are observed (Fig. 5) at the shallowest coastal site closest to Nuuk (Appendix C), which is under the influence of meltwater from glacial fjords.

Replicate ROV push cores were collected at certain sites to evaluate any consistent change in pore water DSi with time when the sediment cores were left standing onboard at ambient temperature. Results show only minor discrepancies in pore water DSi: up to ± 60 μM when the sampling was carried out on paired replicate cores within 3 h of each other (Fig. 5); this is likely due to spatial heterogeneity in sediments and pore waters. In contrast, when pore water sampling was carried out on paired replicate cores more than 10 h apart from each other, there are greater discrepancies with higher DSi values measured in the pore water sampled later in time (Fig. 5). Our results suggest that pore water in the upper core depths might not reflect original DSi values if the sampling is carried out more than 10 h after retrieval of the sediment core.

4. Discussion

Our multi-disciplinary framework allows a nuanced understanding of the whole silica cycle in this climatically critical region, and specifically, the impact of glacial meltwater in shelf seas and into the open ocean. We are able to address questions surrounding the amount of meltwater reaching the ocean, the mechanism by which it does so, and identify mechanisms for how the meltwater is entrained in coastal and boundary currents. For the main context of this study, we can then use this information to understand better the implications of meltwater inputs on macronutrient distributions and biological production, in particular the supply and uptake of DSi. Lastly, we use our palaeoclimate archives to interrogate past changes in meltwater supplies, which are likely to have had a major impact on nutrient cycling.

4.1. Bathymetric features and their role in shelf-water dynamics

The shipboard bathymetric and backscatter data provided a rapid insight into the geomorphology of the study regions. The bathymetry features, resulting from their glacial history, are likely to be an important influence on modern shelf-water dynamics and biogeochemical cycling. The bathymetric grids obtained off the West Greenland coast include the dedicated surveys offshore Nuuk, Narsaq and Cape Farewell, in addition to data collected along the transits (Fig. 6). They illustrate a wealth of geomorphological features typical of glaciated margins, such as cross-shelf troughs, iceberg ploughmarks, gully systems, submarine canyons and submarine landslides (Dowdeswell, Canals, Jakobsson, Todd, Dowdeswell et al., 2016). Most notably off Nuuk, the inshore-deepening Gothåb (Nuuk) Trough, previously described by Ryan et al. (2016), is likely to be important in driving instabilities in localised circulation, influencing the mixing of melt and glacially derived material into the shelf waters. The trough harbours a number of drumlins, elongated features typical of glacial weathering, in addition to intricate patterns of iceberg ploughmarks at the shallow trough mouth (Fig. 6). Systems of gullies and submarine canyons can be found at both the Gothåb and Narsaq trough-mouth fans, and along the shelf edge (Fig. 6). Some of the canyons are cut up to 350 m into the continental slope, and feature steep to near-vertical walls along their flanks together with scoured channels at their floors. Offshore Narsaq,

Table 1

End-member values used in the mass balance calculations.

	Irminger	Meteoric	Sea ice
Salinity	34.88	0	3
$\delta^{18}O$ (‰)	+0.34	c. −21	Surface values +2.1

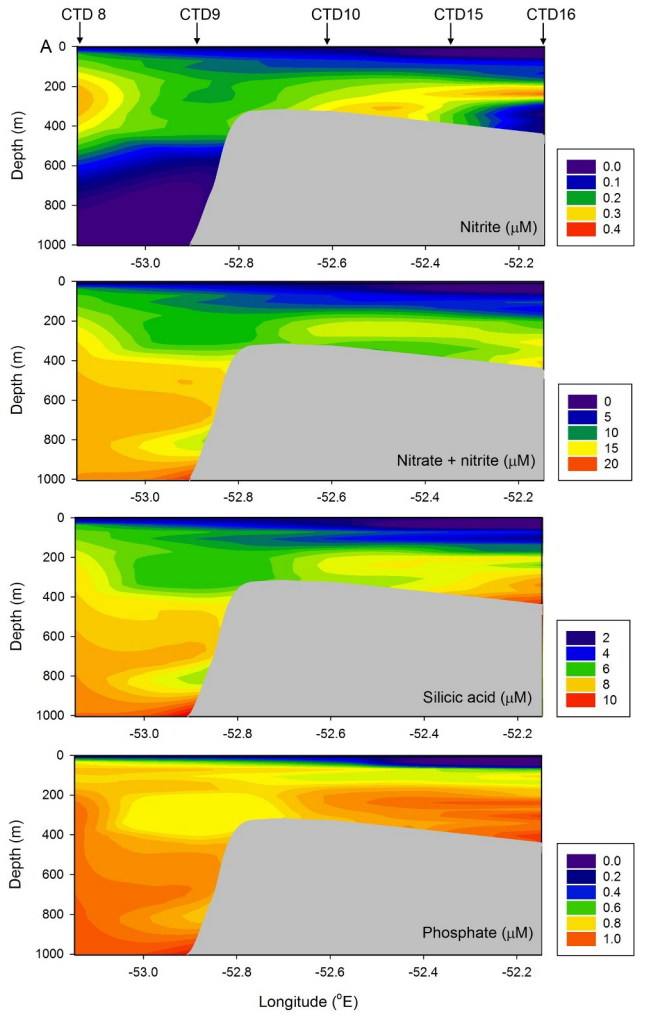

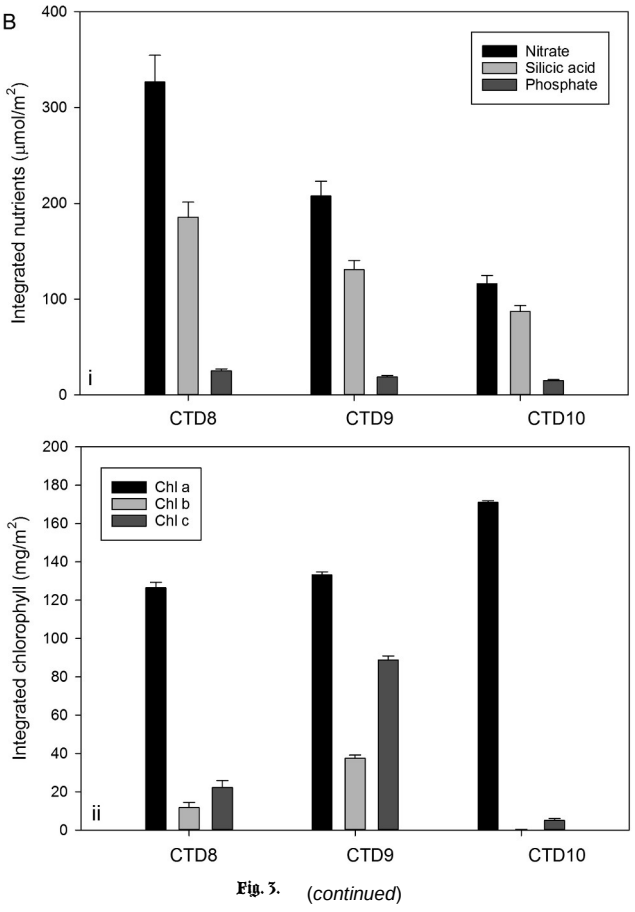

Fig. 3. (A) Example cross section of macronutrient concentrations from the Nuuk grid (from CTD 8 to CTD 16), showing (from top to bottom): nitrite, nitrate, silicic acid, and phosphate (all in μM). This section crosses the shelf break and occupied the prominent glacial trough, as shown in Fig. 2. (B) Example cross section of integrated (top 50 m) macronutrient and algal pigment concentrations from the Nuuk grid (from CTD 8 to CTD 10, see Fig. 2). (i) Integrated macronutrients; (ii) Integrated pigment concentrations. Error bars show propagated errors on integration calculation (± 1SD).

some of the submarine canyons appear to have evolved as a result of retrogressive failures cutting upslope along gullies (Fig. 6).

4.2. Physical tracers of glacial meltwater inputs, mixing and advection

We can use the gridded hydrographic and geostrophic velocity fields to constrain the flow of water across the shelf break, focusing on the Gothåb (Nuuk) Trough CTD section (Fig. 2b). The subsurface temperature minimum indicates the core of Polar Surface Water, whilst the subsurface temperature maximum is Irminger Water. The Irminger Water is present between 200 m and 700 m over the continental slope, with a core temperature of 4.9 °C. There are clear traces of this water mass in the trough also, where warm (θ > 4 °C) and saline (S > 34.7) water is observed near the bottom at CTD16 and CTD10. The Polar Surface Water core is spread across the whole section at 50–150 m, with minimum temperatures recorded at the station furthest onshore (CTD16).

Geostrophic velocities were calculated by referencing the geostrophic shear to the velocity field measured directly with a Lowered Acoustic Doppler Current Profiler (LADCP). The LADCP velocity field was de-tided, by subtracting the barotropic tide solution obtained from the Oregon State University (OSU) model (Egbert and Erofeeva, 2002). The resultant geostrophic velocity field reveals two surface intensified current cores, one on each side of the trough mouth (Fig. 7). The offshore core is associated with a hydrographic front around 15 km west of the shelf break and extends down beyond 400 m depth. Its offshore location is consistent with the long-term average position of the West Greenland Current (Myers et al., 2009).

The inshore velocity core has a less distinct hydrographic signature and therefore its origin is more uncertain at present. One possibility is that the velocity maximum is the result of topographic steering of the inshore portion of the West Greenland Current by the bathymetric trough. Alternatively, it could represent an eddy of offshore water that has detached from the boundary current. A velocity maximum was also detected in a bathymetric trough inshore of Fylla Bank (near Nuuk) in a numerical model simulation (Myers et al., 2009), but there has been no further study into the nature of this feature to date. Such strong inshore current anomalies have significant consequences for the transport of terrestrially-derived freshwater and nutrients.

In addition to the mean flows, eddies formed from the West Greenland Current transport water from the boundary current to the interior Labrador Sea, where they contribute to the process of Labrador Sea Water formation (Katsman et al., 2004). Baroclinic instability is thought to be a key formation mechanism, and years of enhanced baroclinicity tend to coincide with high eddy activity (Rykova et al., 2015), which transfer hydrographic anomalies into the interior. There is significant baroclinicity in both branches of the WGC in our section, implying that eddy generation may be significant. In addition, wind driven Ekman transport is likely to be a key driver in the export of shelf water across the WGC and into the Labrador Sea interior (Schulze et al., 2018).

Cuny et al. (2002) have suggested that, around this location, the

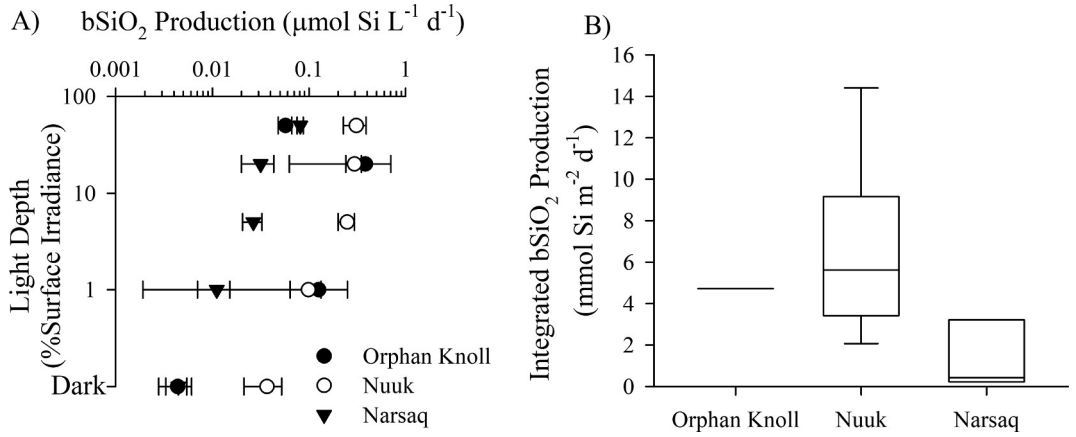

Fig. 4. Biogenic silica ($bSiO_2$) production during ICYLAB. (A) Averaged (± 1SD) gross rates of $bSiO_2$ production (µmol Si L^{-1} d^{-1}) versus relative light depth (i.e. 100% is surface, 1% is base of the euphotic zone) among profiles within Orphan Knoll (filled circles), Nuuk (open circles), and Narsaq (filled triangles). (B) Box plots of euphotic-zone integrated $bSiO_2$ production (mmol Si m^{-2} d^{-1}) for profiles in Orphan Knoll (n = 2), Nuuk (n = 9), and Narsaq (n = 6).

West Greenland Current splits into westward and northward flowing components. However, the location of the splitting, and the partitioning of the water masses involved is not well understood. There are two westward components that flow around the northern perimeter of the Labrador Sea and a northward branch that extends close to the Greenland shelf break (Cuny et al., 2002). Hydrographic signatures of the West Greenland Current have been reported near Greenland to the north, in the vicinity of Davis Strait and Baffin Bay (Cuny et al., 2005; Myers et al., 2009).

4.3. Chemical tracers of glacial inputs

4.3.1. Chemical tracers of meltwater

Vertical sections of sea ice melt and meteoric percentages based on seawater salinity and $\delta^{18}O$ for the Gothåb (Nuuk) Trough CTD section (Fig. 8), reveals a negative offshore gradient in both sea ice melt and meteoric water percentages. Higher freshwater concentrations are found in the trough at all depths, highlighting the potential for glacially-sourced waters to reach the outer shelf and the strong boundary currents.

Freshwater mass balance calculations have, alternatively, been carried out in the High Arctic using salinity and alkalinity endmembers resulting in robust meteoric water percentage reconstructions (e.g. Hendry et al., 2018; Jones et al., 2008). We compared the two mass balance methods using DY081 data, using both a high meteoric water alkalinity endmember typical of the riverine input to the Arctic Ocean (Jones et al., 2008), and a lower meteoric water alkalinity endmember typical of glacial meltwater (Meire et al., 2015). Our comparison indicates that – irrespective of the endmember values chosen - alkalinity-derived values of meteoric water percentages are impacted by subsurface processes that show correlations with nitrite concentrations and temperature (Appendix C). Such non-conservative behaviour likely arises as a result of enhanced alkalinity flux due to water column nitrification, and/or sedimentary denitrification (Fennel et al., 2008; Wolf-Gladrow et al., 2007).

4.3.2. Geochemical tracers of particulate flux

Radium (Ra) is produced continuously from lithogenic material by the decay of thorium (Th) and thus displays elevated concentrations near any sediment–water interface. Short-lived Ra activities did not show a clear relationship with salinity (Fig. 9), but did exhibit informative regional variability. The relatively low activities around Cape Farewell indicate a lack of recent lithogenic input upstream of this region (along the eastern coast of Greenland). From Cape Farewell $^{224}Ra_{XS}$ increases westwards to ~51° W, consistent with increasing cumulative sedimentary inputs into the Greenland coastal current (Fig. 9C). As CTD profiles show that the shallow surface mixed layer sampled by our towfish extended to only 10–20 m, the most likely sources for $^{224}Ra_{XS}$ are glacial meltwater, very shallow sediments within fjords, or resuspended shelf sediments by storm-driven mixing. This signal then decreases towards Nuuk, which will reflect both dilution due to mixing and decay of the short-lived isotope (half-life 3.66 d), and also suggests minimal further lithogenic input into the surface mixed layer. The difference in activity from ~9 dpm m^{-3} at ~51° W to < 4.5 dpm m^{-3} at the Nuuk sampling stations suggests a decay time of one half-life between these sampling regions, a distance of 300–400 km, although dilution or additional inputs would also affect the measured activity and cannot be fully quantified at present. However, the maximum $^{224}Ra_{XS}$ activities of 8–9 dpm m^{-3} above deep water off the shelf break demonstrate that this lithogenic signal is persistent, with the potential to rapidly transport other glacial and sedimentary-derived compounds far offshore.

Although this spatial pattern is not clear in the longer-lived $^{223}Ra_{XS}$ (Fig. 9B), the lower overall activity of this isotope - as well as lower detection efficiency - lead to lower signal to noise ratios. It is also likely that regional lithologies may lead to different input patterns due to differing distribution of the ^{227}Ac and ^{228}Th parents.

Our analysis also quantifies ^{228}Th, the parent of ^{224}Ra. Due to its lithogenic origin and higher particle reactivity, trends in ^{228}Th may be more closely associated with particulate phases than Ra, especially in our unfiltered samples. Samples collected on fibre are generally assumed to retain the majority of both particulate and dissolved Th, although in coastal waters this approach may underestimate total ^{228}Th where particles can be flushed through the sample, and the activities presented here also include supported activity from ^{228}Ra (the parent of ^{228}Th) within the water column. Nevertheless, our ^{228}Th data (Fig. 9D) shows a statistically significant correlation with salinity. We therefore suggest that contrasting patterns in the $^{224}Ra_{XS}$ daughter may be attributed to additional inputs from fjord or shallow shelf sediments, as these inputs are more significant for dissolved species. Additional samples from inner fjord locations and depths below the mixed layer will enable us to differentiate between inputs from marine and glacial sediments.

4.4. Diatom productivity in glacially-influenced shelf seas

Despite the low nutrient concentrations, $bSiO_2$ production rates were significant in the meltwater influenced waters off the shelf and slope. Similar surface DSi concentrations are observed in the open-ocean gyres (e.g. North Pacific, Brzezinski et al. (2011); North Atlantic, Krause et al. (2010)) and typically do not support high rates of diatom productivity. Spring-season $bSiO_2$ production rates in Svalbard and the

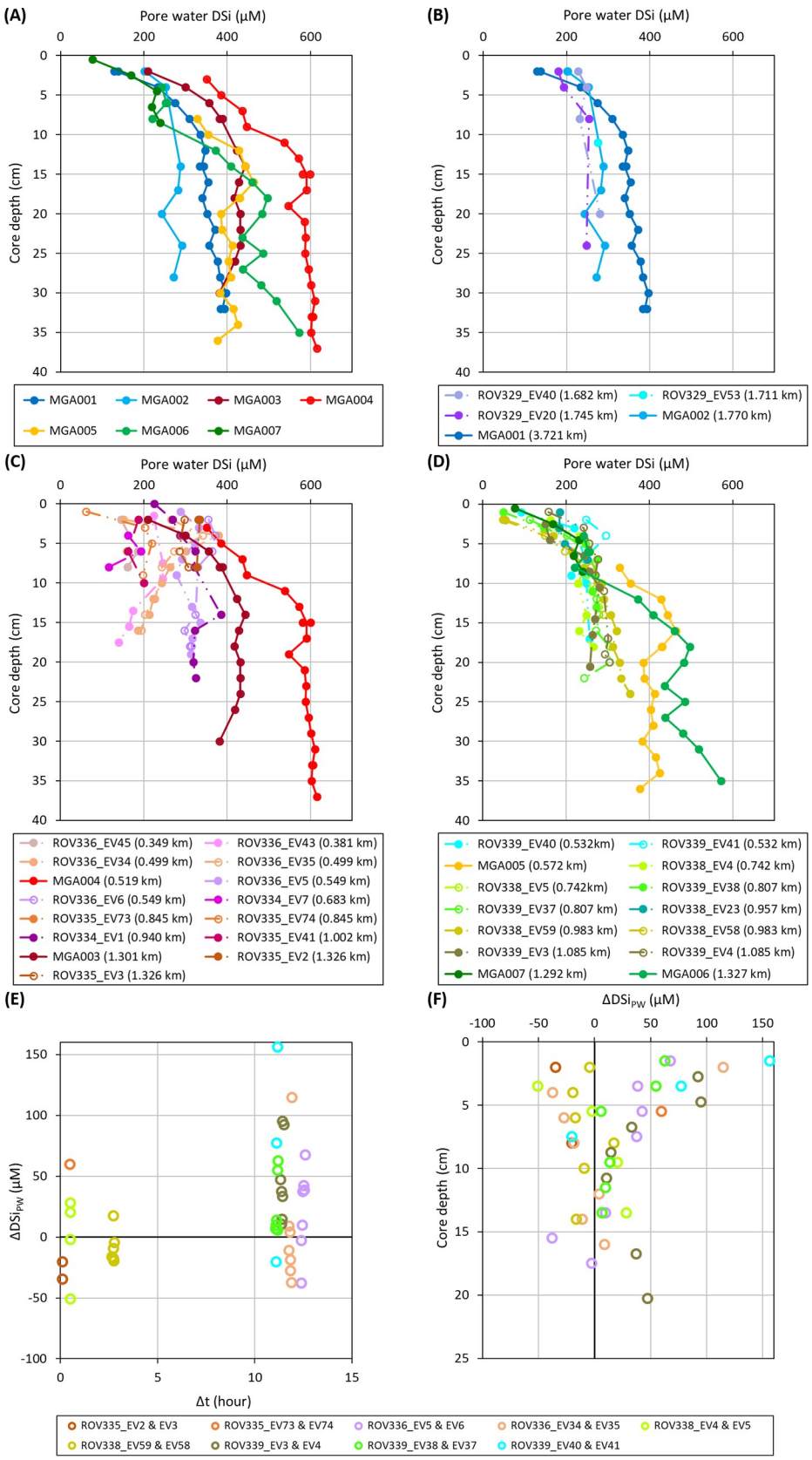

Fig. 5. Pore water dissolved silicon concentration (DSi) measurements versus mega core (MGA, solid lines) or ROV push core (dash-dot lines) depths. Results from (a) mega cores, (b) Orphan Knoll cores, (c) cores off Nuuk, and (d) cores off Narsaq and Cape Farewell. Empty circles are results from replicate push cores retrieved at certain sites. Bracketed numbers in plot legends indicate water depths of the sediment cores. Differences in pore water dissolved silicon concentration between replicate push cores that were sampled at different time periods (ΔDSiPW). ΔDSiPW was calculated by subtracting push core pore water DSi sampled at the latter time period from the corresponding replicate push core pore water DSi sampled at the earlier time period. The calculation was carried out between measurements from the same or nearby (≤ ± 1 cm) sediment core depths. (e) ΔDSiPW versus the time difference between the sampling periods of the replicate cores (Δt), (f) ΔDSiPW versus core depth.

Barents Sea (Krause et al., 2018) and at the MarineBasis Nuuk station in Godthaabsfjord (Krause et al., 2019) were routinely lower than those quantified at Orphan Knoll or Nuuk. The active production below the euphotic zone suggests either recently exported diatoms (e.g. from surface waters within 1–2 days) or the presence of siliceous and active Rhizaria (Biard et al., 2018; Biard et al., 2016). Integrated $bSiO_2$ production rates in the euphotic zone ranged two orders of magnitude, 0.13–14.4 mmol Si m^{-2} d^{-1}. Four of the six stations off Southern

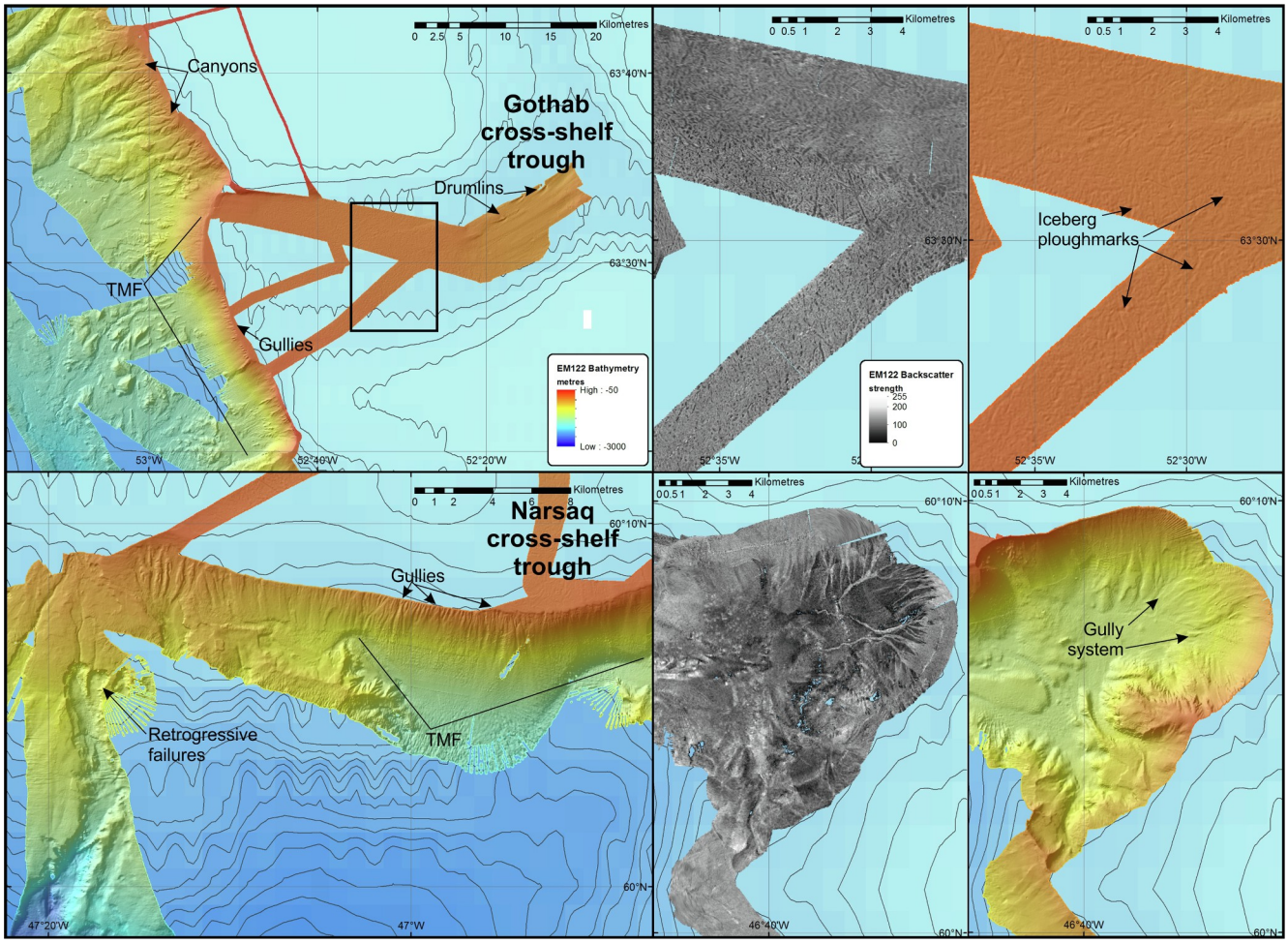

Fig. 6. Examples of submarine glacial landforms offshore W Greenland identified in the shipboard multibeam data. Background: bathymetry from ETOPO5 (www.ngdc.noaa.gov/mgg/global/etopo5.HTML), contour interval 100 m. Location of maps indicated on Fig. 1. TMF: trough-mouth fan.

Greenland had integrated rates < 1 mmol Si m^{-2} d^{-1}, similar to mid-ocean gyres (Brzezinski et al., 2011), whereas all other profiles during the cruise exceeded 2 mmol Si m^{-2} d^{-1}. These rates are on the lower end for the Southern Ocean (1–93 mmol Si m^{-2} d^{-1}, Nelson et al. (1995)) but are similar to Svalbard and the Barents Sea during spring (0.3–1.5 mmol Si m^{-2} d^{-1}, Krause et al. 2018). Overall, diatom $bSiO_2$ production consumed 4% (median) – 10% (average) of the euphotic zone DSi inventory daily. These data are the first such reports for this region of the Labrador Sea and Greenland, and demonstrate a surprisingly active diatom assemblage despite low nutrients, temperature, and biomass.

4.5. Influence of glacial meltwaters in the open ocean: Si cycling as a case study

Although glacial meltwaters exhibit elevated concentrations of some dissolved nutrients and reactive phases (e.g. Hawkings et al., 2017), glacial fjords – the conduits between the source of these nutrients and the open ocean – are characterised by complex physical, chemical and biological processes and are highly variable in space and time (Hopwood et al., 2018). Despite the highly heterogeneous nature of these environments, we can use the findings from DY081 to shed more light on the key common processes that characterise the transfer of nutrients across the land-ocean interface, which will likely vary in rates and importance between different glaciated regions.

In many high-latitude regions, upwelled waters are thought to dominate the supply of nutrients to the euphotic zone supporting most of the primary production. For example, off the West Antarctic Peninsula (WAP), biological “hotspots” were thought to be fed by upwelling Circumpolar Deep Water (CDW) being channelled onto the shelf via glacially carved canyons (Schofield et al., 2013). However, there is increasing evidence that CDW is heavily modified as it transits onto the shelf likely due to a flux of silica and iron from shallow marine sediments (Henley et al., 2018; Sherrell et al., 2018). However, even in these relatively nutrient-rich environments, there is still some important direct input from glacial meltwaters (e.g. Annett et al., 2015) due to the release of reactive phases and promotion of biological mediation of nutrient cycling through the formation of organic matter and biogenic minerals.

Despite different boundary conditions compared to the WAP, similar processes are likely to be happening in glaciated regions of SW Greenland. For example, elevated DSi (> 20 μM) in Greenlandic fjords measured in surface waters (Hawkings et al., 2017) cannot simply be explained by mixing between the freshwater and marine end-members: these concentrations are higher than the freshwater endmember, and there are no seawater masses with sufficiently high DSi concentrations in the top 100 m to supply this flux (Fig. 3, see also Appendix C). The fjord water must be modified – in an analogous way to the WAP – likely by particle-water interactions, including the release of DSi from reactive phases derived from glacial weathering products, or biogenic silica (Hawkings et al., 2018; Hawkings et al., 2017; Meire et al., 2016). This modification may be active in the water column, as well as at the sediment-water interface, in the fjords as well as in the shallow water shelf-sediments (Fig. 5).

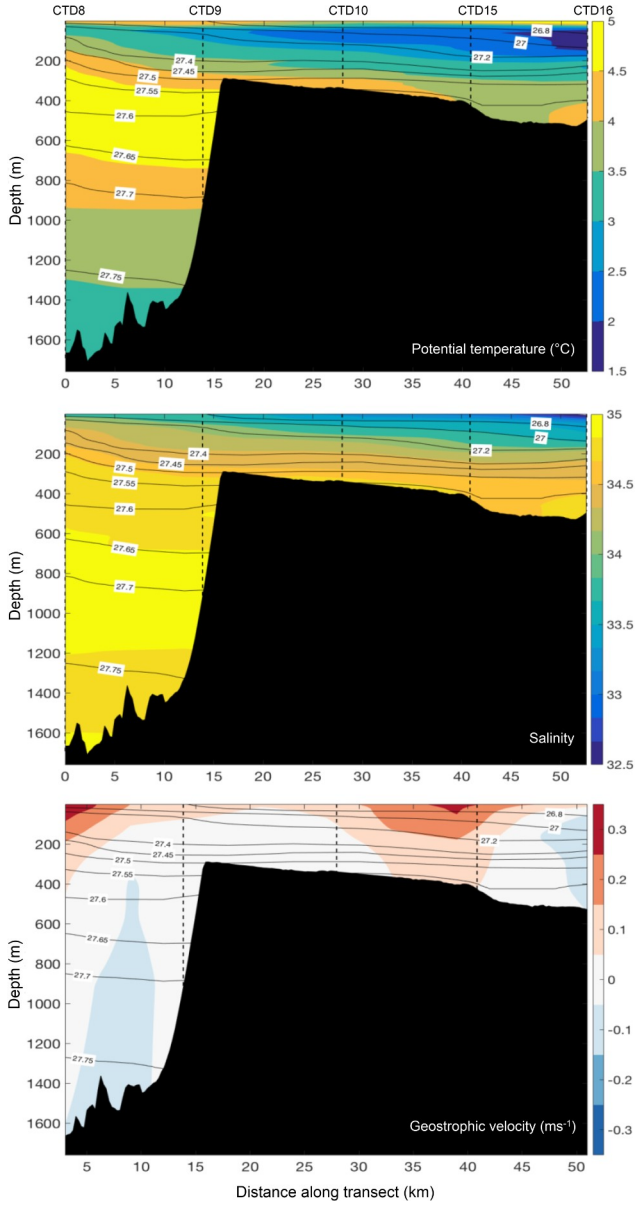

Fig. 7. Gridded vertical sections, from top to bottom, of potential temperature (°C), salinity, and geostrophic velocity (m s $^{-1}$) along Gothåb (Nuuk) Trough. The direction of geostrophic flow is perpendicular to the CTD section (positive northward and negative southward). The black lines with the white boxed labels are isopycnals, which are lines of constant potential density (in kg m $^{-3}$). The dashed vertical lines indicate the CTD stations, labelled at the top of each panel, from which these vertical sections were derived.

However, despite this enrichment within the fjord, the low-salinity waters reaching the coastal ocean are low in DSi as a result of uptake mechanisms that are active as the fjordic waters reach the shelf; our forthcoming studies of uptake kinetics and algal physiology from within the fjords themselves will elucidate whether biological uptake is playing a key role in Si cycling in these regions. Although there is apparently a limited supply of DSi exported from fjords, there appears to be active cycling of silica by diatoms in coastal waters. Our findings show the potential for meteoric waters, and glacially-derived particles, to be exported as far as the coastal and boundary currents, and into the open ocean, where further processing could act to release bioavailable elements. Whilst some of these exported particles may dissolve within the water column during sinking, some will reach the sediment-water interface. Pore water DSi can be used to evaluate the chemical changes of the sediments post-deposition such as the dissolution of this reactive glacial material in addition to dissolution of biogenic silica remains of diatoms and sponges, secondary or 'reverse' weathering, and the recycling of DSi back to the bottom waters (Rahman et al., 2017). The high, but variable, DSi concentrations found in the pore waters at our coastal study sites point towards high rates of benthic regeneration fluxes. Calculated sedimentary diffusive fluxes off SW Greenland, using the approach of Ragueneau et al. (2001), range from 0.1 to 0.3 mmol Si m^{-2} d^{-1}, and are at least 10% of the diatom production rates. Our findings suggest that the total DSi flux across the sediment-water interface, including from advective processes, could rival the magnitude of water column biogenic silica production rates. The high uptake rates of diatoms, together with this rapid recirculation of DSi across the sediment-water interface, points towards a silica cycle maintained by strong pelagic-benthic coupling.

4.6. Approaches to reconstructing glacial meltwater inputs through time

Glacial meltwaters are enriched in both dissolved and particulate nutrients, including silicon, and our new data highlight that these meltwaters extend across the shelf into boundary currents. In the context of the marine silicon cycle, our data show that, whilst DSi reaching the shelf waters from the glacial fjords may be low, diatom activity is surprisingly high. DSi must be reaching the surface, potentially by mixing with modified shelf waters. Our Ra isotopic data (Section 4.3.2) reveal that there is input of glacial particles into these shelf waters, potentially via sediment reworking, which may contribute bioavailable silicon via dissolution both in the water column and at the sediment-water interface. This system is likely to be sensitive to glacial inputs, and so quantifying changes in meltwater fluxes through time - using a variety of climate archives - is going to be key to understanding shelf and slope productivity during past episodes of climatic change.

4.6.1. Fossil deep-sea corals

The geochemistry of fossil skeletons of deep-sea corals has the potential to record aspect of past environmental conditions (Chen et al., 2016; Robinson et al., 2014). In particular, water masses distribution and food supply are thought to be important for deep-sea coral populations off the West Greenland margin. Given their environmental sensitivity, cold-water coral distributions are likely to susceptible to changes in water mass properties and primary production caused by meltwater inputs. In 2017, the first living samples of the cold-water scleractinian coral, *Lophelia pertusa*, were collected from approximately 60°22′N off the Greenland within a layer of relatively warm, modified Atlantic Water (Kenchington et al., 2017).

We have now been able to make in situ observations of cold water corals off Greenland, as well as showing that corals have been present on the Greenland Margin for at least 10,000 years (Fig. 10). These first populations likely appeared with melting of the large ice fields of the last glacial period. Supporting prior research, we also found that scleractinian corals have been present further south on Orphan Knoll for at least 130,000 years (Fig. 10; Cao et al., 2007; Hillaire-Marcel et al., 2017). In both locations our suite of dates show that the populations have not been stable. This observation implies shifts in environmental pressures over these timescales, likely driven by a shift in balance between warmer Atlantic waters and cold meltwater-rich polar waters.

4.6.2. Marine sediments and past glacial meltwater inputs

During the last ice age, catastrophic iceberg discharge events episodically flooded the subpolar North Atlantic with meltwater (Heinrich, 1988). Evidence suggests that these "Heinrich events" (Broecker et al., 1992), were related to, and may have acted as the trigger for (Broecker, 2003; Clark et al., 2002), dramatic changes in ocean circulation (McManus et al., 2004) and heat distribution that were felt globally (e.g. Wang et al., 2001). In addition to global impacts, changes in ice

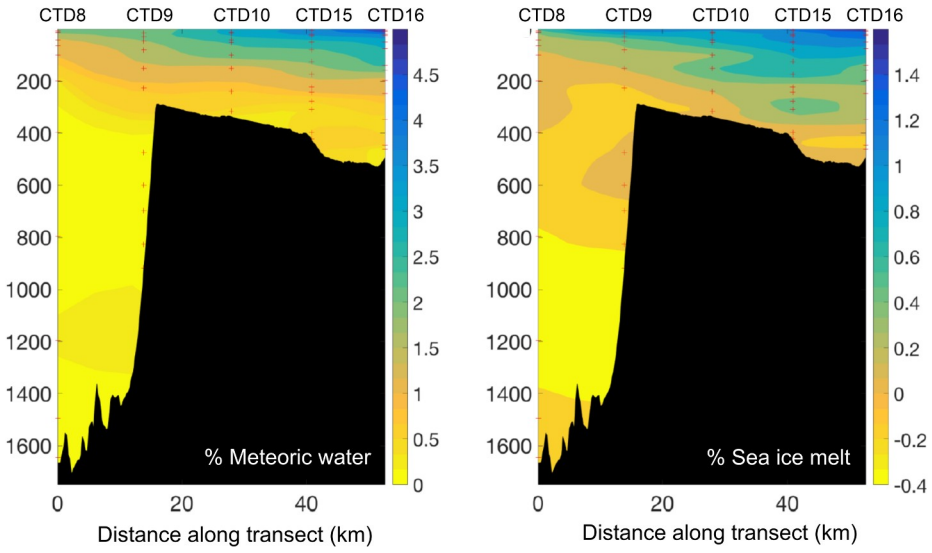

Fig. 8. Vertical sections of meteoric water and sea ice melt percentages along Gothåb (Nuuk) Trough. The black area is the bathymetry of the section, as measured by the ship multibeam. Red pluses indicate the bottle sampling locations, with the CTD stations annotated above. (For interpretation of the references to colour in this figure legend, the reader is referred to the web version of this article.)

sheet dynamics and meltwater inputs would also have had considerable impacts on more regional biogeochemical cycling. While previous work has identified the existence of eight such events over the last 70 ka (Andrews et al., 1995; Bond et al., 1992; Bond and Lotti, 1995; Rashid et al., 2003; Stoner et al., 1996), questions remain about the origin(s) of these events, their trigger(s) and the nature of their primary signatures across the North Atlantic (Andrews and Voelker, 2018). Gravity cores collected at Orphan Knoll (DY081-GVY002 & GVY002), Southwest Greenland (DY081-GVY003) and Cape Farewell (DY081-GVY004 & GVY 005) represent new opportunities to constrain the timing, geometry and character of iceberg discharge and glacial meltwater release in the paleo record.

Existing work on marine sediment cores from the high latitude North Atlantic has employed a variety of proxies to identify pulses of meltwater delivery and associated ice rafted debris delivery. Previously applied proxies include $^{230}Th_{xs,0}$ (to assess changes in sedimentary fluxes (McManus et al., 1998)), counts of IRD and foraminifera (to identify the relative abundance of terrestrially-derived debris and foraminifera (Heinrich, 1988)), foraminifera census (to determine the relative abundance of cold-dwelling planktonic species such as *N. pachyderma s.* (Ruddiman et al., 1977)), $\delta^{18}O$ of *N. pachyderma s.* (to quantify the cooling and/or freshening of surface waters (Bond et al.,

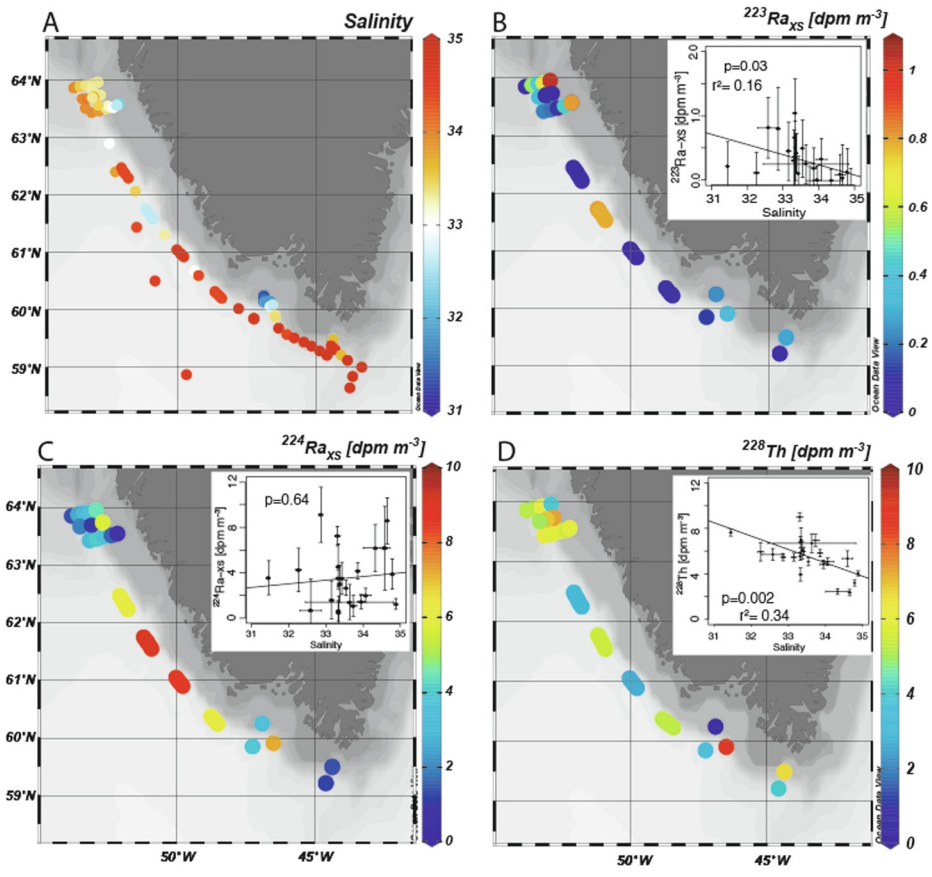

Fig. 9. Spatial distribution of salinity (A), $^{223}Ra_{XS}$ (B) $^{224}Ra_{XS}$ (C) and ^{228}Th (D) from towfish samples taken at 2–5 m depth. Elongated symbols show underway samples which took ~1 h to collect. For B-D, inset plots show the same isotope versus salinity in surface waters. Vertical error bars denote ± 1 standard error for activities, and horizontal error bars show the standard deviation of salinity measurements taken each minute during the ~1 h sampling interval.

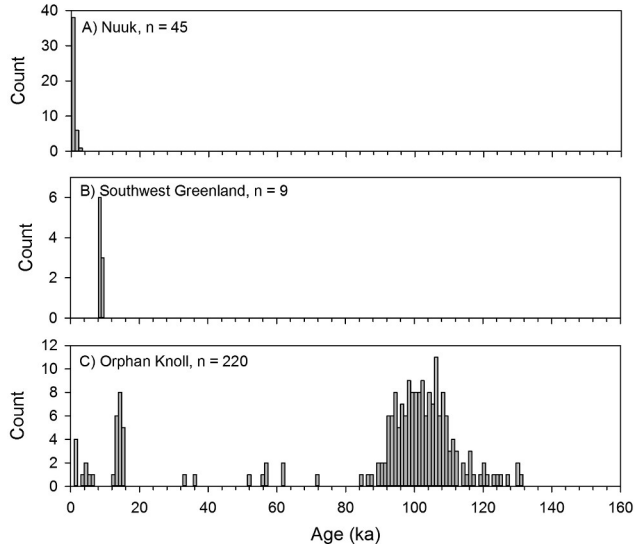

Fig. 10. Uranium-thorium age data for fossil corals collected during DY081.

1993)), magnetic susceptibility (to identify detrital sediment (Grousset et al., 1993)), x-ray diffraction (XRD) (to assess changes in the abundance of quartz and plagioclase feldspar (Moros et al., 2002; Moros et al., 2004)), and X-ray fluorescence (XRF) (to identify changes in sedimentary elemental ratios (Hodell et al., 2008)). Unfortunately, the comparison of sediment core records has been limited by difficulties in establishing tightly constrained chronologies. This has impeded analysis of the triggers of events and the range of their influence (Andrews and Voelker, 2018). While previous work has utilized one or more of the proxy approaches identified above, complete assessment of the proxies described above, in a single core, would greatly assist in interpreting the paleoceanographic record. In addition, despite the widespread inference that icebergs originated from the Laurentide ice sheet during these events (Bond and Lotti, 1995; Broecker, 2003; Hodell et al., 2008; McManus et al., 1998), relatively fewer detailed studies have examined their imprint and consequences in the proximal Labrador Sea (Andrews and Voelker, 2018).

Our goal in analysing the new DY081 cores is to use a wide range of proxies to address temporal relationships and the spatial signatures of Heinrich events. Our findings show that GVY001 (Orphan Knoll) represents a record of continuous sedimentation from 40 to 50 ka to present and likely captures the Younger Dryas and Heinrich events 1–4 (Fig. 11). In GVY001 Heinrich event signatures have been identified in records of IRD counts, the $\delta^{18}O$ of planktonic foraminifera, XRD and XRF scans. These results confirm the utility of using the suite of proxies in DY081 cores to tie together previously incomparable records from sediment cores in which disparate proxies have been applied, to reconstruct meltwater inputs in the region back through time.

5. Synthesis and outlook

Coastal and shelf sea biogeochemical research in the polar regions requires high-resolution spatial and temporal datasets, due to the inherent heterogeneous nature of the high-latitude margin settings. Whilst obtaining the necessary temporal resolution is challenging, especially in the absence of expensive long-term monitoring programs, it is possible to combine traditional physical and biogeochemical measurements with novel isotopic and observational methods that integrate signals over a variety of timescales (days to thousands of years). Stable and radiometric isotope geochemistry also allows the identification of common processes within this highly-variable system, which are active over given timescales. All of these approaches can be combined with palaeoceanographic techniques to obtain a reliable baseline for pre-industrial conditions, and also look for analogues of future change from the past.

In the context of the marine silica cycle, our findings from DY081

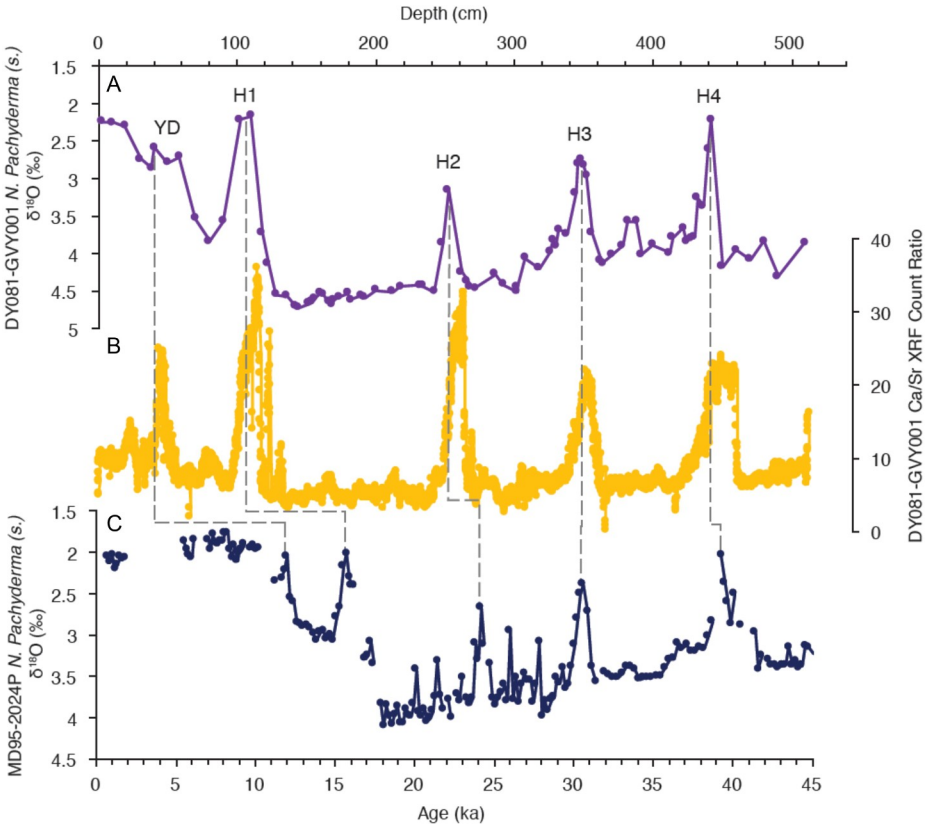

Fig. 11. Proxies for North Atlantic Heinrich Events. (a) *N. Pachyderma* (s.) $\delta^{18}O$ from DY081-GVY001 (purple). (b) Ca/Sr XRF count ratio from DY081-GVY001 (yellow). (c) *N. Pachyderma* (s.) $\delta^{18}O$ (Hillaire-Marcel and Bilodeau, 2000) on the age model of Lynch-Stieglitz et al. (2014) (navy blue). Vertical grey dashes suggest age-depth assignments for DY081-GVY001. (For interpretation of the references to colour in this figure legend, the reader is referred to the web version of this article.)

are able to show that:

- There are strong mean flows that are conducive to eddy generation, which will likely transport freshwater from the margin into the boundary currents that supply the Labrador Sea;
- Oxygen isotopes robustly trace meteoric water composition adjacent to Greenland, with near-surface concentrations of 5% over the shelf reflecting significant glacial discharge;
- Ra isotopes indicate additions of glacial meltwater and sedimentary particulates are spatially heterogeneous and rapidly transported;
- Low macronutrient concentrations (e.g. DSi) are found in coastal waters influenced by glacial melt;
- Diatoms are surprisingly active given the low nutrient availability and low temperature (i.e. consuming 5–10% of euphotic zone Si daily);
- There is a strong benthic flux of DSi from sediments;
- Fossil corals can be used to track changes in benthic ecosystems through time, likely influenced by water mass distribution;
- Sediment cores recovered of sufficient length and resolution to reconstruct meltwater inputs at least back to 45 ka (i.e. Heinrich events 0–4).

Acknowledgments

The authors would like to thank the Captain and crew of the RRS *Discovery*, the National Marine Facility technicians, David Turner, and project manager, Daniel Comben, National Oceanography Centre Southampton (NOCS). Many thanks to Sinhue Torres-Valdes and Christopher D. Coath for assistance in the laboratory, and the Marine Geoscience group at NOCS for providing the core-splitter. Additional thanks to Lorenz Meire and colleagues at the Greenland Institute of Natural Resources. Funding for DY081 was from the European Research Council (ERC Starting Grant 678371 ICY-LAB). The contributions of AWJ, GGC, and JFM were supported in part by the US-NSF.

Appendix A. Supplementary material

Supplementary data to this article can be found online at https://doi.org/10.1016/j.pocean.2019.102126.

References

Alexeev, V.A., Walsh, J.E., Ivanov, V.V., Semenov, V.A., Smirnov, A.V., 2017. Warming in the Nordic Seas, North Atlantic storms and thinning Arctic sea ice. Environ. Res. Lett. 12, 084011.

Andrews, J., Jennings, A.E., Kerwin, M., Kirby, M., Manley, W., Miller, G., Bond, G., MacLean, B., 1995. A Heinrich-like event, H-0 (DC-0): Source (s) for detrital carbonate in the North Atlantic during the Younger Dryas chronozone. Paleoceanography 10, 943–952.

Andrews, J.T., Voelker, A.H., 2018. "Heinrich events"(& sediments): a history of terminology and recommendations for future usage. Quat. Sci. Rev. 187, 31–40.

Annett, A.L., Henley, S.F., Van Beek, P., Souhaut, M., Ganeshram, R., Venables, H.J., Meredith, M.P., Geibert, W., 2013. Use of radium isotopes to estimate mixing rates and trace sediment inputs to surface waters in northern Marguerite Bay, Antarctic Peninsula. Antarct. Sci. 25, 445–456.

Annett, A.L., Skiba, M., Henley, S.F., Venables, H.J., Meredith, M.P., Statham, P.J., Ganeshram, R.S., 2015. Comparative roles of upwelling and glacial iron sources in Ryder Bay, coastal western Antarctic Peninsula. Mar. Chem. 176, 21–33.

Arrigo, K.R., van Dijken, G.L., Castelao, R.M., Luo, H., Rennermalm, Å.K., Tedesco, M., Mote, T.L., Oliver, H., Yager, P.L., 2017. Melting glaciers stimulate large summer phytoplankton blooms in southwest Greenland waters. Geophys. Res. Lett. 44, 6278–6285.

Bamber, J., Tedstone, A., King, M., Howat, I., Enderlin, E., van den Broeke, M., Noel, B., 2018. Land ice freshwater budget of the Arctic and North Atlantic Oceans: 1. Data, methods, and results. J. Geophys. Res. Oceans 123, 1827–1837.

Berthelsen, T., 2014. Coastal fisheries in Greenland. KNAPK report, Nuuk.

Bhatia, M.P., Kujawinski, E.B., Das, S.B., Breier, C.F., Henderson, P.B., Charette, M.A., 2013. Greenland meltwater as a significant and potentially bioavailable source of iron to the ocean. Nat. Geosci. 6, 274.

Biard, T., Krause, J.W., Stukel, M.R., Ohman, M.D., 2018. The significance of giant phaeodarians (Rhizaria) to biogenic silica export in the California current ecosystem. Global Biogeochem. Cycles.

Biard, T., Stemmann, L., Picheral, M., Mayot, N., Vandromme, P., Hauss, H., Gorsky, G., Guidi, L., Kiko, R., Not, F., 2016. In situ imaging reveals the biomass of giant protists in the global ocean. Nature 532, 504.

Bond, G., Broecker, W., Johnsen, S., McManus, J., Labeyrie, L., Jouzel, J., Bonani, G., 1993. Correlations between climate records from North Atlantic sediments and Greenland ice. Nature 365, 143.

Bond, G., Heinrich, H., Broecker, W.S., Labeyrie, L.D., McManus, J., Andrews, J.E., Huon, S., Jantschik, R., Clasen, S., Simet, C., Tedesco, K., Klas, M., Bonani, G., Ivy, S., 1992. Evidence for massive discharges of icebergs into the North Atlantic ocean during the last glacial period. Nature 360, 245–249.

Bond, G.C., Lotti, R., 1995. Iceberg discharges into the North Atlantic on millenial time scales during the last glaciation. Science 267, 1005–1010.

Broecker, W.S., 2003. Does the trigger for abrupt climate change reside in the ocean or in the atmosphere? Science 300, 1519–1522.

Broecker, W.S., Bond, G.C., Klas, M., Clark, E., McManus, J., 1992. Origin of the northern Atlantic's Heinrich events. Clim. Dyn. 6, 265–273.

Brzezinski, M.A., Krause, J.W., Church, M.J., Karl, D.M., Li, B., Jones, J.L., Updyke, B., 2011. The annual silica cycle of the North Pacific subtropical gyre. Deep Sea Res. Part I 58, 988–1001.

Cao, L., Fairbanks, R.G., Mortlock, R.A., Risk, M.J., 2007. Radiocarbon reservoir age of high latitude North Atlantic surface water during the last deglacial. Quatern. Sci. Rev. 26 (5-6), 732–742.

Carmack, E.C., Yamamoto-Kawai, M., Haine, T.W., Bacon, S., Bluhm, B.A., Lique, C., Melling, H., Polyakov, I.V., Straneo, F., Timmermans, M.L., 2016. Freshwater and its role in the Arctic Marine System: Sources, disposition, storage, export, and physical and biogeochemical consequences in the Arctic and global oceans. J. Geophys. Res. Biogeosci. 121, 675–717.

Chen, T., Robinson, L.F., Beasley, M.P., Claxton, L.M., Andersen, M.B., Gregoire, L.J., Wadham, J., Fornari, D.J., Harpp, K.S.J.S., 2016. Ocean mixing and ice-sheet control of seawater 234U/238U during the last deglaciation. Science 354, 626–629.

Clark, P.U., Pisias, N.G., Stocker, T.F., Weaver, A.J., 2002. The role of the thermohaline circulation in abrupt climate change. Nature 415, 863.

Cuny, J., Rhines, P.B., Kwok, R., 2005. Davis Strait volume, freshwater and heat fluxes. Deep Sea Res. Part I 52, 519–542.

Cuny, J., Rhines, P.B., Niiler, P.P., Bacon, S., 2002. Labrador Sea boundary currents and the fate of the Irminger Sea Water. J. Phys. Oceanogr. 32, 627–647.

Dodd, P.A., Heywood, K.J., Meredith, M.P., Naveira-Garabato, A.C., Marca, A.D., Falkner, K.K., 2009. Sources and fate of freshwater exported in the East Greenland Current. Geophys. Res. Lett. 36.

Dowdeswell, J.A., Canals, M., Jakobsson, M., Todd, B., Dowdeswell, E.K., Hogan, K., 2016. The variety and distribution of submarine glacial landforms and implications for ice-sheet reconstruction. Geol. Soc. Lond. Mem. 46, 519–552.

Egbert, G.D., Erofeeva, S.Y., 2002. Efficient inverse modeling of barotropic ocean tides. J. Atmos. Oceanic Technol. 19, 183–204.

Enderlin, E.M., Howat, I.M., Jeong, S., Noh, M.J., Van Angelen, J.H., Van Den Broeke, M.R., 2014. An improved mass budget for the Greenland ice sheet. Geophys. Res. Lett. 41, 866–872.

Felikson, D., Bartholomaus, T.C., Catania, G.A., Korsgaard, N.J., Kjær, K.H., Morlighem, M., Noël, B., Van Den Broeke, M., Stearns, L.A., Shroyer, E.L., 2017. Inland thinning on the Greenland ice sheet controlled by outlet glacier geometry. Nat. Geosci. 10, 366.

Fennel, K., Wilkin, J., Previdi, M., Najjar, R., 2008. Denitrification effects on air-sea CO2 flux in the coastal ocean: simulations for the northwest North Atlantic. Geophys. Res. Lett. 35.

Grousset, F., Labeyrie, L., Sinko, J., Cremer, M., Bond, G., Duprat, J., Cortijo, E., Huon, S., 1993. Patterns of ice-rafted detritus in the glacial North Atlantic (40–55° N). Paleoceanography 8, 175–192.

Hawkings, J., Wadham, J., Tranter, M., Telling, J., Bagshaw, E., Beaton, A., Simmons, S.L., Chandler, D., Tedstone, A., Nienow, P., 2016. The Greenland Ice Sheet as a hot spot of phosphorus weathering and export in the Arctic. Global Biogeochem. Cycles 30, 191–210.

Hawkings, J.R., Hatton, J.E., Hendry, K.R., de Souza, G.F., Wadham, J.L., Ivanovic, R., Kohler, T.J., Stibal, M., Beaton, A., Lamarche-Gagnon, G., 2018. The silicon cycle impacted by past ice sheets. Nat. Commun. 9, 3210.

Hawkings, J.R., Wadham, J.L., Benning, L.G., Hendry, K.R., Tranter, M., Tedstone, A., Nienow, P., Raiswell, R., 2017. Ice sheets as a missing source of silica to the polar oceans. Nat. Commun. 8, 14198.

Hawkings, J.R., Wadham, J.L., Tranter, M., Raiswell, R., Benning, L.G., Statham, P.J., Tedstone, A., Nienow, P., Lee, K., Telling, J., 2014. Ice sheets as a significant source of highly reactive nanoparticulate iron to the oceans. Nat. Commun. 5.

Heinrich, H., 1988. Origin and consequences of cyclic ice rafting in the northeast Atlantic Ocean during the past 130,000 years. Quat. Res. 29, 142–152.

Hendry, K.R., 2017. RRS discovery cruise DY081, July 6th – August 8th 2017. National Marine Facilities.

Hendry, K.R., Pyle, K.M., Barney Butler, G., Cooper, A., Fransson, A., Chierici, M., Leng, M.J., Meyer, A., Dodd, P.A., 2018. Spatiotemporal variability of barium in arctic sea-ice and seawater. J. Geophys. Res.: Oceans.

Henley, S.F., Jones, E.M., Venables, H.J., Meredith, M.P., Firing, Y.L., Dittrich, R., Heiser, S., Stefels, J., Dougans, J., 2018. Macronutrient and carbon supply, uptake and cycling across the Antarctic Peninsula shelf during summer. Phil. Trans. R. Soc. A 376, 20170168.

Hillaire-Marcel, C., Bilodeau, G., 2000. Instabilities in the Labrador Sea water mass structure during the last climatic cycle. Can. J. Earth Sci. 37, 795–809.

Hillaire-Marcel, C., Maccali, J., Ménabréaz, L., Ghaleb, B., Blénet, A., Edinger, E., 2017. U-series vs 14C ages of deep-sea corals from the southern Labrador Sea: Sporadic development of corals and geochemical processes hampering estimation of ambient water ventilation ages. In: EGU General Assembly Conference Abstracts, Vol. 19, pp.

9126.
Hodell, D.A., Channell, J.E., Curtis, J.H., Romero, O.E., Röhl, U., 2008. Onset of "Hudson Strait" Heinrich events in the eastern North Atlantic at the end of the middle Pleistocene transition (~ 640 ka)? Paleoceanography 23.
Hopwood, M.J., Bacon, S., Arendt, K., Connelly, D., Statham, P., 2015. Glacial meltwater from Greenland is not likely to be an important source of Fe to the North Atlantic. Biogeochemistry 124, 1–11.
Hopwood, M.J., Carroll, D., Browning, T.J., Meire, L., Mortensen, J., Krisch, S., Achterberg, E.P., 2018. Non-linear response of summertime marine productivity to increased meltwater discharge around Greenland. Nat. Commun. 9, 3256.
Jones, E., Anderson, L., Jutterström, S., Swift, J., 2008. Sources and distribution of fresh water in the East Greenland Current. Prog. Oceanogr. 78, 37–44.
Katsman, C.A., Spall, M.A., Pickart, R.S., 2004. Boundary current eddies and their role in the restratification of the Labrador Sea. J. Phys. Oceanogr. 34, 1967–1983.
Kenchington, E., Yashayaev, I., Tendal, O.S., Jørgensbye, H., 2017. Water mass characteristics and associated fauna of a recently discovered Lophelia pertusa (Scleractinia: Anthozoa) reef in Greenlandic waters. Polar Biol. 40, 321–337.
Krause, J.W., Brzezinski, M.A., Jones, J.L., 2011. Application of low-level beta counting of 32Si for the measurement of silica production rates in aquatic environments. Mar. Chem. 127, 40–47.
Krause, J.W., Duarte, C.M., Marquez, I.A., Assmy, P., Fernández-Méndez, M., Wiedmann, I., Wassmann, P., Kristiansen, S., Agustí, S., 2018. Biogenic silica production and diatom dynamics in the Svalbard region during spring. Biogeosciences 15, 6503–6517.
Krause, J.W., Nelson, D.M., Lomas, M.W., 2010. Production, dissolution, accumulation, and potential export of biogenic silica in a Sargass Sea mode-water eddy. Limnol. Oceanogr. 55, 569–579.
Krause, Jeffrey W., Schulz, Isabelle K., Rowe, Katherine A., Dobbins, William, Winding, Mie H.S., Sejr, Mikael K., Duarte, Carlos M., Agustí, Susana, 2019. Silicic acid limitation drives bloom termination and potential carbon sequestration in an Arctic bloom. Sci. Rep. 9.
Kuzyk, Z.Z.A., Gobeil, C., Goñi, M.A., Macdonald, R.W., 2017. Early diagenesis and trace element accumulation in North American Arctic margin sediments. Geochim. Cosmochim. Acta 203, 175–200.
Lindsay, R., Schweiger, A., 2015. Arctic sea ice thickness loss determined using subsurface, aircraft, and satellite observations. The Cryosphere 9, 269–283.
Luo, H., Castelao, R.M., Rennermalm, A.K., Tedesco, M., Bracco, A., Yager, P.L., Mote, T.L., 2016. Oceanic transport of surface meltwater from the southern Greenland ice sheet. Nat. Geosci. 9, 528.
Lynch-Stieglitz, J., Schmidt, M.W., Henry, L.G., Curry, W.B., Skinner, L.C., Mulitza, S., Zhang, R., Chang, P., 2014. Muted change in Atlantic overturning circulation over some glacial-aged Heinrich events. Nat. Geosci. 7, 144.
Maslanik, J., Fowler, C., Stroeve, J., Drobot, S., Zwally, J., Yi, D., Emery, W., 2007. A younger, thinner Arctic ice cover: increased potential for rapid, extensive sea-ice loss. Geophys. Res. Lett. 34.
McManus, J.F., Anderson, R.F., Broecker, W.S., Fleisher, M.Q., Higgins, S.M., 1998. Radiometrically determined sedimentary fluxes in the sub-polar North Atlantic during the last 140,000 years. Earth Planet. Sci. Lett. 155, 29–43.
McManus, J.F., Francois, R., Gherardi, J.-M., Keigwin, L.D., Brown-Leger, S., 2004. Collapse and rapid resumption of Atlantic meridional circulation linked to deglacial climate changes. Nature 428, 834–837.
Meire, L., Meire, P., Struyf, E., Krawczyk, D., Arendt, K., Yde, J., Juul Pedersen, T., Hopwood, M.J., Rysgaard, S., Meysman, F., 2016. High export of dissolved silica from the Greenland Ice Sheet. Geophys. Res. Lett. 43, 9173–9182.
Meire, L., Mortensen, J., Meire, P., Juul-Pedersen, T., Sejr, M.K., Rysgaard, S., Nygaard, R., Huybrechts, P., Meysman, F.J., 2017. Marine-terminating glaciers sustain high productivity in Greenland fjords. Glob. Change Biol. 23, 5344–5357.
Meire, L., Søgaard, D., Mortensen, J., Meysman, F., Soetaert, K., Arendt, K., Juul-Pedersen, T., Blicher, M., Rysgaard, S., 2015. Glacial meltwater and primary production are drivers of strong CO2 uptake in fjord and coastal waters adjacent to the Greenland Ice Sheet. Biogeosciences 12, 2347–2363.
Melling, H., Moore, R.M., 1995. Modification of halocline source waters during freezing on the Beaufort Sea shelf: evidence from oxygen isotopes and dissolved nutrients. Cont. Shelf Res. 15, 89–113.
Meredith, M., Heywood, K., Dennis, P., Goldson, L., White, R., Fahrbach, E., Schauer, U., Østerhus, S., 2001. Freshwater fluxes through the western Fram Strait. Geophys. Res. Lett. 28, 1615–1618.
Meredith, M.P., Brandon, M.A., Wallace, M.I., Clarke, A., Leng, M.J., Renfrew, I.A., van Lipzig, N.P.M., King, J.C., 2008. Variability in the freshwater balance of northern Marguerite Bay, Antarctic Peninsula: results from d ^{18}O. Deep-Sea Res. II 55, 309–322.
Moore, W.S., 2008. Fifteen years experience in measuring 224Ra and 223Ra by delayed-coincidence counting. Mar. Chem. 109, 188–197.
Moore, W.S., Arnold, R., 1996. Measurement of 223Ra and 224Ra in coastal waters using a delayed coincidence counter. J. Geophys. Res. Oceans 101, 1321–1329.
Moros, M., Kuijpers, A., Snowball, I., Lassen, S., Bäckström, D., Gingele, F., McManus, J.J.M.G., 2002. Were glacial iceberg surges in the North Atlantic triggered by climatic warming? Mar. Geol. 192, 393–417.
Moros, M., McManus, J., Rasmussen, T., Kuijpers, A., Dokken, T., Snowball, I., Nielsen, T., Jansen, E., 2004. Quartz content and the quartz-to-plagioclase ratio determined by X-ray diffraction: a proxy for ice rafting in the northern North Atlantic? Earth Planet. Sci. Lett. 218, 389–401.
Myers, P.G., Donnelly, C., Ribergaard, M.H., 2009. Structure and variability of the West Greenland Current in Summer derived from 6 repeat standard sections. Prog. Oceanogr. 80, 93–112.
Nelson, D.M., Treguer, P., Brzezinski, M.A., Leynaert, A., Queguiner, B., 1995. Production and dissolution of biogenic silica in the ocean: revised global estimates, comparison with regional data and relationship to biogenic sedimentation. Global Biogeochem. Cycles 9, 359–372.
Oliver, H., Luo, H., Castelao, R.M., van Dijken, G.L., Mattingly, K.S., Rosen, J.J., Mote, T.L., Arrigo, K.R., Rennermalm, Å.K., Tedesco, M., 2018. Exploring the potential impact of Greenland meltwater on stratification, photosynthetically active radiation, and primary production in the labrador sea. J. Geophys. Res. Oceans 123, 2570–2591.
Proshutinsky, A., Dukhovskoy, D., Timmermans, M.-L., Krishfield, R., Bamber, J.L., 2015. Arctic circulation regimes. Phil. Trans. R. Soc. A 373, 20140160.
Provost, C., Sennéchael, N., Miguet, J., Itkin, P., Rösel, A., Koenig, Z., Villacieros-Robineau, N., Granskog, M.A., 2017. Observations of flooding and snow-ice formation in a thinner Arctic sea ice regime during the N-ICE2015 campaign: Influence of basal ice melt and storms. J. Geophys. Res. Oceans.
Ragueneau, O., Gallinari, M., Corrin, L., Grandel, S., Hall, P., Hauvespre, A., Lampitt, R., Rickert, D., Stahl, H., Tengberg, A., 2001. The benthic silica cycle in the Northeast Atlantic: annual mass balance, seasonality, and importance of non-steady-state processes for the early diagenesis of biogenic opal in deep-sea sediments. Prog. Oceanogr. 50, 171–200.
Rahman, S., Aller, R., Cochran, J., 2017. The missing silica sink: revisiting the marine sedimentary Si cycle using cosmogenic 32Si. Global Biogeochem. Cycles.
Rashid, H., Hesse, R., Piper, D.J., 2003. Evidence for an additional Heinrich event between H5 and H6 in the Labrador Sea. Paleoceanography, 18.
Robinson, L.F., Adkins, J.F., Frank, N., Gagnon, A.C., Prouty, N.G., Roark, E.B., van de Flierdt, T., 2014. The geochemistry of deep-sea coral skeletons: a review of vital effects and applications for palaeoceanography. Deep Sea Res. Part II: Top. Stud. Oceanogr. 99, 184–198.
Ruddiman, W.F., Sancetta, C., McIntryre, A., 1977. Glacial/interglacial response rate of subpolar North Atlantic waters to climatic change: the record in oceanic sediments. Phil. Trans. R. Soc. Lond. B 280, 119–142.
Ryan, J., Dowdeswell, J., Hogan, K., 2016. Three cross-shelf troughs on the continental shelf of SW Greenland from Olex data. Geol. Soc. Lond. Mem. 46, 167–168.
Rykova, T., Straneo, F., Bower, A.S., 2015. Seasonal and interannual variability of the West Greenland Current System in the Labrador Sea in 1993–2008. J. Geophys. Res. Oceans 120, 1318–1332.
Schofield, O., Ducklow, H., Bernard, K., Doney, S., Patterson-Fraser, D., Gorman, K., Martinson, D., Meredith, M., Saba, G., Stammerjohn, S., 2013. Penguin biogeography along the West Antarctic Peninsula: testing the canyon hypothesis with Palmer LTER observations. Oceanography 26, 204–206.
Schulze, L.M., Frajka-Williams, E., 2018. Wind-driven transport of fresh shelf water into the upper 30m of the Labrador Sea. Ocean Sci. 14 (5), 1247–1264.
Sherrell, R.M., Annett, A.L., Fitzsimmons, J.N., Roccanova, V.J., Meredith, M.P., 2018. A 'shallow bathtub ring'of local sedimentary iron input maintains the Palmer Deep biological hotspot on the West Antarctic Peninsula shelf. Phil. Trans. R. Soc. A 376, 20170171.
Stoner, J.S., Channell, J.E., Hillaire-Marcel, C., 1996. The magnetic signature of rapidly deposited detrital layers from the deep Labrador Sea: relationship to North Atlantic Heinrich layers. Paleoceanogr. Paleoclimatol. 11, 309–325.
Thomas, H., Shadwick, E., Dehairs, F., Lansard, B., Mucci, A., Navez, J., Gratton, Y., Prowe, F., Chierici, M., Fransson, A., 2011. Barium and carbon fluxes in the Canadian Arctic Archipelago. J. Geophys. Res. Oceans 116.
Van As, D., Andersen, M.L., Petersen, D., Fettweis, X., Van Angelen, J.H., Lenaerts, J.T., Van Den Broeke, M.R., Lea, J.M., Bøggild, C.E., Ahlstrøm, A.P., 2014. Increasing meltwater discharge from the Nuuk region of the Greenland ice sheet and implications for mass balance (1960–2012). J. Glaciol. 60, 314–322.
van den Broeke, M., Box, J., Fettweis, X., Hanna, E., Noël, B., Tedesco, M., van As, D., van de Berg, W.J., van Kampenhout, L., 2017. Greenland ice sheet surface mass Loss: recent developments in observation and modeling. Curr. Climate Change Rep. 3, 345–356.
Wadham, J.L., Hawkings, J., Telling, J., Chandler, D., Alcock, J., Lawson, E., Kaur, P., Bagshaw, E., Tranter, M., Tedstone, A., 2016. Sources, cycling and export of nitrogen on the Greenland Ice Sheet. Biogeosci. Discuss.
Wang, Y.-J., Cheng, H., Edwards, R.L., An, Z., Wu, J., Shen, C.-C., Dorale, J.A., 2001. A high-resolution absolute-dated late Pleistocene monsoon record from Hulu Cave, China. Science 294, 2345–2348.
Weatherdon, L.V., Magnan, A.K., Rogers, A.D., Sumaila, U.R., Cheung, W.W., 2016. Observed and projected impacts of climate change on marine fisheries, aquaculture, coastal tourism, and human health: an update. Front. Mar. Sci. 3, 48.
Wolf-Gladrow, D.A., Zeebe, R.E., Klaas, C., Körtzinger, A., Dickson, A.G.J.M.C., 2007. Total alkalinity: the explicit conservative expression and its application to biogeochemical processes. Mar. Chem. 106, 287–300.
Yang, Q., Dixon, T.H., Myers, P.G., Bonin, J., Chambers, D., Van Den Broeke, M., Ribergaard, M.H., Mortensen, J., 2016. Recent increases in Arctic freshwater flux affects Labrador Sea convection and Atlantic overturning circulation. Nature Commun. 7 ncomms10525.